SIAM J. Applied Dynamical Systems
Vol. 9, No. 2, pp. 611–633

Localized Instability and Attraction along Invariant Manifolds*

George Haller† and Themistoklis Sapsis‡

Abstract. We derive a simple criterion for transverse instabilities along a general invariant manifold of a multi-dimensional dynamical system. The criterion requires an appropriately defined normal infinitesimal Lyapunov exponent (NILE) to be positive over regions of transverse instability on the manifold. Unlike classic Lyapunov-type numbers in the theory of normally hyperbolic invariant manifolds, the NILE can be computed analytically in applications. This enables us to locate, for example, regions of transient jumping along an invariant manifold that is otherwise globally attracting. To illustrate our results, we determine the locations of intermittent instabilities in bubble motion past a cylinder, in predator-prey interactions, and in soft-stiff structural systems.

Key words. normal stability of invariant manifolds, slow manifold reduction, local instabilities along invariant manifolds, infinitesimal Lyapunov exponents

AMS subject classifications. 37D05, 37D10, 37D25

DOI. 10.1137/08074324X

1. Introduction.

Invariant manifolds are distinguished sets of trajectories that organize the global geometry of trajectories in a dynamical system. The stability type of an invariant manifold can be determined from asymptotic Lyapunov-type numbers introduced by Fenichel [3].

Calculating Lyapunov-type numbers requires the explicit knowledge of nonlinear solutions on the manifold; it also involves the computation of the linearized flow along individual trajectories on the manifold. As a result, an analytic calculation of the Lyapunov-type numbers is realistic only for simple or near-integrable systems. In typical applications, the Lyapunov-type numbers have to be determined numerically along each trajectory on the manifold.

Even if an invariant manifold is attracting (i.e., all close enough trajectories ultimately converge to the manifold), it may admit localized regions of instability where nearby trajectories temporarily depart from the manifold. These departures and later returns may manifest themselves in spectacular jumps along the manifold. Such transient jumps are often important to locate in applications, even though asymptotic Lyapunov-type numbers carry no information about these jumps.

For example, for neutrally buoyant finite-size particles (suspensions) in a fluid, the equations of motion admit a globally attracting invariant manifold that can be found analytically

*Received by the editors December 10, 2008; accepted for publication (in revised form) by M. Dellnitz March 25, 2010; published electronically June 9, 2010. This research was supported by AFOSR grants FA 9550-06-0092 and FA 9550-06-1-0101 and by a George and Marie Vergottis Fellowship at MIT.
http://www.siam.org/journals/siads/9-2/74324.html
†Department of Mechanical Engineering, McGill University, Montreal, QC H3A 2K6, Canada (george.haller@mcgill.ca).
‡Department of Mechanical Engineering, Massachusetts Institute of Technology, Cambridge, MA 02139 (sapsis@mit.edu).

(Babiano et al. [1]). The dynamics on this inertial manifold coincides with the dynamics of the ambient fluid; thus suspension dynamics are expected to synchronize with fluid particle dynamics rapidly. Recent studies, however, revealed that suspension particles tend to disperse around, rather than converge to, the motion of infinitesimal fluid particles (Babiano et al. [1]). Sapsis and Haller [13] showed that this dispersion is due to repeated transverse jumps of trajectories over unstable regions of the inertial manifold.

Detecting local instabilities along an invariant manifold is also helpful for another reason: a global loss of stability along an invariant manifold is always preceded by the appearance of local instabilities. Specifically, a global loss of stability on an otherwise robust invariant manifold takes place when the set of local instabilities becomes sizeable enough to contain a sufficiently large subset of at least one ω-limit set on the manifold. An example of this phenomenon is the soft-stiff mechanical system analyzed by Georgiou, Corless, and Bajaj [5], as we shall see in section 6.3.

In this work, we extend the ideas from the specialized setting considered in Sapsis and Haller [13] (specific dynamical system; planar invariant manifold; linear dynamics transverse to the manifold) to identify localized transverse instability and attraction on general invariant manifolds. Our main tool in achieving this is the normal infinitesimal Lyapunov exponent (NILE), defined as the leading order short-term stretching or contraction rate at points of an invariant manifold.

We derive a general explicit formula for the NILE and hence for the normally stable and unstable domains of an invariant manifold. We discuss the application of our results to three problems involving local instabilities along invariant manifolds: bubble dynamics in flow past a cylinder, oscillations of predator-prey interactions, and soft-stiff structural systems.

A comment is in order on the relation of the present work to the stability of Lagrangian coherent structures (LCSs), i.e., finite-time repelling or attracting invariant manifolds in the dynamics of infinitesimally small fluid particles (cf. Haller and Yuan [6]; Haller [7]). When applied to a known LCS, our present results reveal the instantaneous localized stability properties of the LCS from Eulerian strain-type quantities, such as those featured in the statement of Theorem 4. Computing these quantities along the LCS at any point in time does not involve the long-term integration of individual particle trajectories. Locating the LCSs themselves in an unsteady fluid flow, however, requires the application of Lagrangian tools and hence the integration of particles over an extended period of time. To describe the local stability of LCSs, therefore, ultimately requires a combination of Lagrangian and Eulerian methods.

2. Set-up and definitions.

Consider a dynamical system of the form

$$\dot{X} = \mathcal{F}(X,t), \qquad X \in \mathbb{R}^n, \tag{1}$$

with $n \geq 2$, and with a smooth function $\mathcal{F}\colon \mathbb{R}^n \times \mathbb{R} \to \mathbb{R}^n$. A trajectory $X(t;t_0,X_0)$ of this system is a solution of the initial value problem $X(t_0) = X_0$. The flow map associated with (1) is a two-parameter family of transformations defined as

$$\begin{aligned} F_{t_0}^t &: \mathbb{R}^n \to \mathbb{R}^n, \\ &X_0 \mapsto X(t;t_0,X_0). \end{aligned}$$

The linearized flow map $DF_{t_0}^t$ is defined as

$$DF_{t_0}^t : T\mathbb{R}^n \to T\mathbb{R}^n,$$
$$(p, v) \mapsto \left(F_{t_0}^t(p), D_{X_0}X(t; t_0, p)v\right),$$

mapping vectors v based at a point p to vectors $D_{X_0}X(t; t_0, p)v$ based at the point $F_{t_0}^t(p)$. The notation $T\mathbb{R}^n$ refers to the tangent bundle of $\mathbb{R}^n$; a local fiber of this bundle at a point $p \in \mathbb{R}^n$ will be denoted by $T_p\mathbb{R}^n$.

We assume that $M(t) \subset \mathbb{R}^n$ is a k-dimensional differentiable manifold that is locally invariant over / under the map $F_{t_0}^t$ over the time interval $[t_1, t_2]$. This means that

$$F_{t_0}^t(M(t_0)) \subset M(t) \tag{2}$$

for all times $t_0, t \in [t_1, t_2]$ with $t \geq t_0$.

Beyond invariance and smoothness, we make no further assumption about the manifold $M(t)$. We do note that $M(t)$ will typically only be of interest in physical applications if it is robust, i.e., persists under small perturbations. As Fenichel [3] showed, such persistence is ensured if $M(t)$ is time-independent, compact, and normally hyperbolic.

3. Normally stable and normally unstable subsets. Instead of the asymptotic behavior along $M(t)$, our focus here is on the instantaneous behavior of trajectories close to $M(t)$. Specifically, we would like to locate points on $M(t)$ at which most transverse perturbations to $M(t)$ start growing in norm over infinitesimally short times. (A measure zero set of transverse perturbations is allowed to decrease at such points due to the presence of stable directions.) The union of such points will form the *normally unstable subset* $M_u(t)$ of $M(t)$. Similarly, the *normally stable subset* $M_s(t)$ of $M(t)$ is the union of points in $M(t)$ at which all transverse perturbations to $M(t)$ decay over infinitesimally short times.

Note that $M_s(t)$ and $M_u(t)$ are typically not invariant subsets of $M(t)$: trajectories in $M(t)$ will generally either avoid both of these subsets or simply cross them. Likewise, trajectories near $M(t)$ may either stay away from the subsets $M_s(t)$ and $M_u(t)$ of $M(t)$ or pass over these regions. In the latter case, however, the passing trajectories will break away from $M(t)$ while near $M_u(t)$ and approach $M(t)$ while near $M_s(t)$ (see Figure 1).

If $M_s(t) \equiv M(t)$, then $M(t)$ is a normally hyperbolic locally invariant manifold that admits only stable normal directions; in this case, $M(t)$ has an n-dimensional stable manifold (or domain of attraction). If $M_u(t) \equiv M(t)$, then $M(t)$ is a normally hyperbolic locally invariant manifold that admits only unstable normal directions; in this case, $M(t)$ has an n-dimensional unstable manifold.

The stable and unstable subsets described above have a major impact on the dynamics near $M(t)$. As it turns out below, locating them is possible from explicit calculations, and hence they offer a feasible alternative to Lyapunov-type numbers in the analysis of impact of $M(t)$ on phase space geometry. We make these ideas more precise below.

Definition 1. *Let $T_pM(t)$ and $N_pM(t)$ denote the tangent and normal spaces of $M(t)$ at $p \in M(t)$, respectively. Also, let*

$$\Pi_p^t : T_p\mathbb{R}^n = T_pM(t) \oplus N_pM(t) \to N_pM(t),$$
$$(u, v) \mapsto v$$

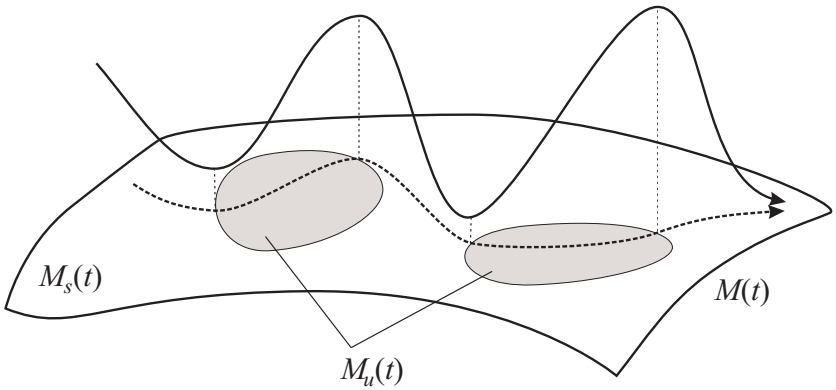

Figure 1. *Trajectories jump away from $M(t)$ over the unstable subset $M_u(t)$ but return to $M(t)$ over the stable subset $M_s(t)$. The figure assumes that $M(t)$ is a normally hyperbolic attracting manifold, in which case the jumping trajectory keeps approaching the same underlying trajectory on $M(t)$ by the invariant foliation of the stable manifold $W^s(M(t))$.*

denote the natural projection from $T_p\mathbb{R}^n$, the tangent space of $\mathbb{R}^n$ at p, to $N_pM(t)$. We then define the normal infinitesimal Lyapunov exponent (NILE) at a point $p \in M(t)$ as

$$\sigma(p;t) = \lim_{s\to+0} \frac{1}{s} \log \left\| \Pi^{t+s}_{F_t^{t+s}(p)} DF_t^{t+s} \Big|_{N_pM(t)} \right\|. \tag{3}$$

The limit in the definition of $\sigma(p;t)$ exists for any v by the differentiability of the linearized flow map $DF^t_{t_0}$ and of the normal projection $\Pi^t_{F^t_{t_0}(p)}$ in t. Also note that the limit is finite because $DF^t_t \equiv I$ by definition, and hence $DF_t^{t+s} - I = \mathcal{O}(s)$. The action of the operator $\Pi^{t+s}_{F_t^{t+s}(p)} DF_t^{t+s}$ on a vector $v_0 \in N_pM(t)$ is shown in Figure 2.

Next, we want to argue that exponent $\sigma(p;t)$ is independent of the choice of the transverse bundle in which we seek to measure growth rates from $M(t)$. To describe this independence in more precise terms, we let $\tilde{N}M(t)$ be another smoothly varying n-dimensional vector bundle that is a fibration over $M(t)$; we require this bundle to be transverse to $M(t)$, by which we mean $\tilde{N}_pM(t) \pitchfork T_pM(t)$ within $T_p\mathbb{R}^n$ for all $p \in M(t)$.

We can then view $T_p\mathbb{R}^n$ as the direct sum of $\tilde{N}_pM(t)$ and $T_pM(t)$,

$$T_p\mathbb{R}^n = \tilde{N}_pM(t) \oplus T_pM(t),$$

and define the natural projection from $T_p\mathbb{R}^n$ onto $\tilde{N}_pM(t)$ as

$$\begin{aligned} \tilde{\Pi}^t_p \colon T_p\mathbb{R}^n = T_pM(t) \oplus \tilde{N}_pM(t) &\to \tilde{N}_pM(t), \\ (\tilde{u}, \tilde{v}) &\mapsto \tilde{v}. \end{aligned}$$

We require each fiber $\tilde{N}_pM(t)$ to have the same constant position relative to the tangent space $T_pM(t)$ and the normal space $N_pM(t)$. Specifically, we require $\tilde{N}M(t)$ to be such that the tangential projection from $\tilde{N}_pM(t)$ to $N_pM(t)$,

$$\begin{aligned} Q \colon \tilde{N}_pM(t) &\to N_pM(t), \\ Q &= \Pi^t_p | \tilde{N}_pM(t), \end{aligned} \tag{4}$$

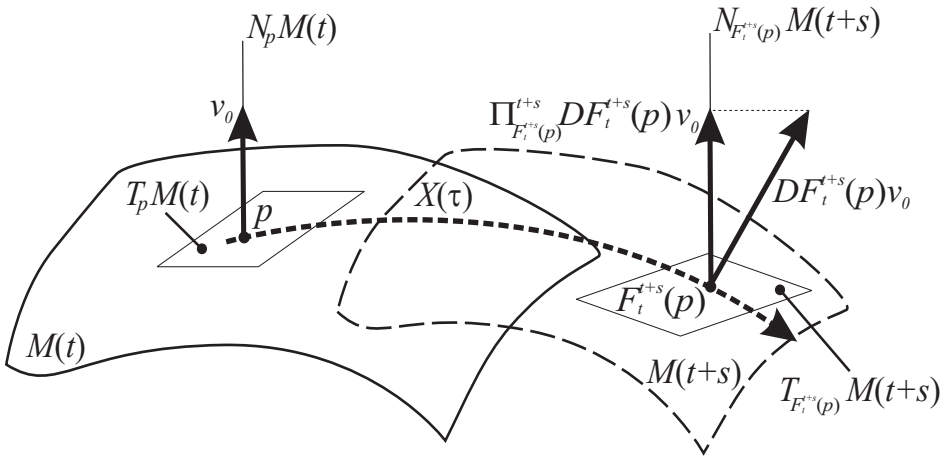

Figure 2. *The operator* $\Pi^{t+s}_{F_t^{t+s}(p)} DF_t^{t+s}|_{N_pM(t)}$ *maps vectors in the normal space* $N_pM(t)$ *to vectors in the normal space* $N_{F_t^{t+s}(p)}M(t+s)$. *The NILE* $\sigma(p;t)$ *is the exponential rate at which the norm of the above operator grows in the limit of infinitesimally small* s. *Therefore,* $\sigma(p;t)$ *measures the exponential rate at which the normal component of vectors normal to the manifold* $M(t)$ *grows over very short times. (The time* τ *is arbitrary within the interval* $[t, t+s]$.*)*

is independent of t and p. This latter condition is important; otherwise the value of the NILE computed on $\tilde{N}M(t)$ would be affected by the s-dependence of the fiber family $\tilde{N}_{F_t^{t+s}(p)}M(t+s)$ along the trajectory $F_t^{t+s}(p)$ starting from p at time t.

Proposition 2. *If we define*

$$\tilde{\sigma}(p;t) = \lim_{s\to+0} \frac{1}{s} \log \left\| \tilde{\Pi}^{t+s}_{F_t^{t+s}(p)} DF_t^{t+s}\Big|_{\tilde{N}_pM(t)} \right\|,$$

then we have $\tilde{\sigma}(p;t) \equiv \sigma(p;t)$.

Proof. Note that the tangential projection Q from $\tilde{N}_pM(t)$ to $N_pM(t)$ is a diffeomorphism, and hence Q^{-1} is well defined and satisfies

$$\tilde{\Pi}^t_p = Q^{-1}\Pi^t_p. \tag{5}$$

We will also need the tangential projection from $\tilde{N}_pM(t)$ to $T_pM(t)$, defined as

$$\begin{aligned} P\colon \tilde{N}_pM(t) &\to T_pM(t), \\ P &= I - \Pi^t_p|\tilde{N}_pM(t). \end{aligned}$$

Note that P is independent of t and p, which follows from (4).

For any $\tilde{v} \in \tilde{N}_pM(t)$, we have

$$\begin{aligned} \tilde{\Pi}^{t+s}_{F_t^{t+s}(p)} DF_t^{t+s}\tilde{v} &= \tilde{\Pi}^{t+s}_{F_t^{t+s}(p)} DF_t^{t+s}\left(Q\tilde{v} + P^t_p\tilde{v}\right) \\ &= \tilde{\Pi}^{t+s}_{F_t^{t+s}(p)} DF_t^{t+s} Q\tilde{v} \\ &= Q^{-1}\Pi^{t+s}_{F_t^{t+s}(p)} DF_t^{t+s} Q\tilde{v}, \end{aligned} \tag{6}$$

where we used the fact that $DF_t^{t+s}\,P_p^t\tilde{v} \in T_pM(t+s)$ by the invariance of the tangent bundle of $M(t)$ under the linearized flow map. We conclude that (cf. (6))

$$\begin{aligned}
\tilde{\sigma}(p;t) &= \lim_{s\to+0}\frac{1}{s}\log\left\|\tilde{\Pi}^{t+s}_{F_t^{t+s}(p)}DF_t^{t+s}\Big|_{\tilde{N}_pM(t)}\right\| \\
&= \lim_{s\to+0}\frac{1}{s}\log\left\|Q^{-1}\Pi^{t+s}_{F_t^{t+s}(p)}DF_t^{t+s}Q\Big|_{\tilde{N}_pM(t)}\right\| \\
&= \lim_{s\to+0}\frac{1}{s}\log\left\|Q^{-1}\Pi^{t+s}_{F_t^{t+s}(p)}DF_t^{t+s}Q\Big|_{Q^{-1}N_pM(t)}\right\| \\
&= \lim_{s\to+0}\frac{1}{s}\log\left\|\Pi^{t+s}_{F_t^{t+s}(p)}DF_t^{t+s}\Big|_{N_pM(t)}\right\| \\
&= \sigma(p;t),
\end{aligned}$$

as claimed. ∎

We conclude that the $\sigma(p;t)$ is independent of the choice of transverse directions to the invariant manifold and hence gives an intrinsic characterization of the local stability of $M(t)$ at t. Motivated by this observation, we introduce the following definition of normally stable and unstable subsets of $M(t)$.

Definition 3. *We define the normally unstable subset of $M(t)$ as*

$$M_u(t) = \{p \in M \;\mid\; \sigma(p;t) > 0\}$$

and the normally stable subset of $M(t)$ as

$$M_s(t) = \{p \in M \;\mid\; \sigma(p;t) < 0\}.$$

The subsets $M_u(t)$ and $M_s(t)$, described informally above, are now defined precisely through the Lyapunov-type number $\sigma(p;t)$. Unlike the Lyapunov-type numbers arising in Fenichel's theory, however, $\sigma(p;t)$ turns out to be computable explicitly. Consequently, $M_u(t)$ and $M_s(t)$ can be identified in any application, provided the invariant manifold $M(t)$ is known to exist.

4. Computing the NILE. In this section, we give two alternative expressions that can be used for computing the NILE in specific examples. The first expression will assume the explicit knowledge of normal vectors along the manifold $M(t)$. The resulting form of the NILE reveals that, in the language of mechanics, $\sigma(p,t)$ is equal to the maximal normal rate of strain relative to $M(t)$ at the point $p \in M(t)$.

The second expression will utilize a local coordinate representation of $M(t)$. In appropriate coordinates $(x,y) \in \mathbb{R}^k \times \mathbb{R}^{n-k}$, the k-dimensional invariant manifold $M(t)$ can always be written locally as a smooth graph:

$$M(t) = \Big\{(x,y) \in \mathbb{R}^k \times \mathbb{R}^{n-k} : y = \varphi(x,t), \quad x \in D(t)\Big\}, \qquad t \in [t_1,t_2]; \tag{7}$$

here $D(t)$ is an open domain on which the local coordinate x is defined at time t (see Figure 3). The vector variable x may contain some parameters (dummy variables) on which the

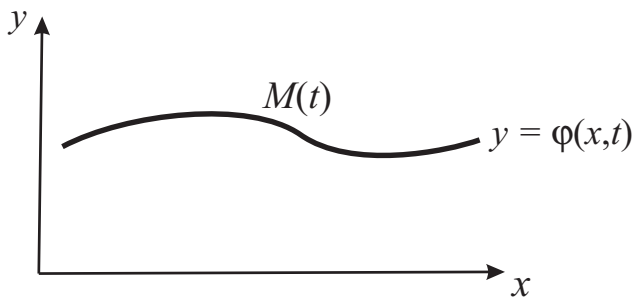

Figure 3. *The manifold $M(t)$ as a local graph over the x variables.*

dynamical system depends; this is why we have suppressed any explicit parameter dependence in (1) and (8).

In the local variables (x, y), the dynamical system (1) takes the form

$$\begin{aligned} \dot{x} &= f(x, y, t), \\ \dot{y} &= g(x, y, t), \end{aligned} \tag{8}$$

where f and g are sufficiently smooth functions of their arguments.

Theorem 4.

(i) *Let $n(p,t)$ be a unit normal vector field to $M(t)$ that is smooth both in $p \in M(t)$ and in t. We then have*

$$\sigma(p,t) = \max_{n(p,t)\in N_p M(t)} \langle n(p,t), D\mathcal{F}(p,t)n(p,t)\rangle,$$

with $\langle \cdot, \cdot \rangle$ denoting the standard Euclidean inner product.

(ii) *Using the local form $y = \varphi(x,t)$ of $M(t)$ and the vector field (8), we define the matrix field*

$$\Gamma(x,t) = g_y(x, \varphi(x,t), t) - \varphi_x(x,t)\, f_y(x, \varphi(x,t), t), \tag{9}$$

where the subscript refers to differentiation with respect to the variable in the subscript. We then have

$$\sigma(x,t) = \lambda_{\max}\left[\Gamma(x,t) + \Gamma^T(x,t)\right]/2,$$

where $\lambda_{\max}[\cdot]$ refers to the largest eigenvalue of a symmetric matrix.

Proof. The linearized flow along a trajectory $X(t+s;t,p) \in M(t+s)$ (with initial condition $X(t;t,p) = p$) satisfies

$$\dot{\xi}(t+s) = D\mathcal{F}(X(t+s;t,p), t+s)\xi(t+s), \qquad \xi(t+s) = DF_t^{t+s}(p)\xi(t) \in T_{X(t+s;t,p)}\mathbb{R}^n. \tag{10}$$

Note that $n(p,t)$ has unit length at each point along the trajectory $X(t+s;t,p)$, implying

$$\frac{d}{ds}\langle n(X(t+s;t,p), t+s), n(X(t+s;t,p), t+s)\rangle = 0,$$

or, equivalently,

$$\begin{aligned} &\langle [D_p n(X(t+s;t,p), t+s)\mathcal{F}(X(t+s;t,p), t+s) \\ &+ D_t n(X(t+s;t,p), t+s)], n(X(t+s;t,p), t+s)\rangle = 0. \end{aligned} \tag{11}$$

Selecting the initial condition

$$\xi(t) \equiv n(p,t) \tag{12}$$

for the linear flow (10), we can write the projection of $\xi(t+s)$ on the local unit normal $n(X(t+s;t,p),t+s)$ in the form

$$\begin{aligned}
&\langle n(X(t+s;t,p),t+s),\xi(t+s)\rangle \\
&= \langle n(p,t),\xi(t)\rangle + \frac{d}{ds}\langle n(X(t+s;t,p),t+s),\xi(t+s)\rangle\,|_{s=0}\cdot s + O(s^2) \\
&= 1 + \left\langle n(p,t),\dot{\xi}(t)\right\rangle s + O(s^2) \\
&= 1 + \langle D\mathcal{F}(p,t)n(p,t),n(p,t)\rangle\, s + O(s^2), \qquad (13)
\end{aligned}$$

where we used (11) and (12).

Using (10), (12), and (13), we can compute the NILE as follows:

$$\begin{aligned}
\sigma(p;t) &= \lim_{s\to+0}\frac{1}{s}\log\left\|\Pi^{t+s}_{F_t^{t+s}(p)}DF_t^{t+s}\Big|_{N_pM(t)}\right\| \\
&= \lim_{s\to+0}\frac{1}{s}\log\left|\max_{n(p,t)\in N_pM(t)}\left\langle n(X(t+s;t,p),t+s),DF_t^{t+s}n(p,t)\right\rangle\right| \\
&= \lim_{s\to+0}\frac{1}{s}\log\left|\max_{n(p,t)\in N_pM(t)}\langle n(X(t+s;t,p),t+s),\xi(t+s)\rangle\right| \\
&= \lim_{s\to+0}\frac{1}{s}\log\left|\max_{n(p,t)\in N_pM(t)}\left[1+\langle D\mathcal{F}(p,t)n(p,t),n(p,t)\rangle\, s+O(s^2)\right]\right| \\
&= \lim_{s\to+0}\frac{1}{s}\max_{n(p,t)\in N_pM(t)}\log\left[1+\langle D\mathcal{F}(p,t)n(p,t),n(p,t)\rangle\, s+O(s^2)\right] \\
&= \max_{n(p,t)\in N_pM(t)}\langle D\mathcal{F}(p,t)n(p,t),n(p,t)\rangle,
\end{aligned}$$

which completes the proof of statement (i) of the theorem.

To prove statement (ii), we recall that by Proposition 2, $\sigma(p,t)$ can be computed with respect to any smooth n-dimensional vector bundle $\tilde{N}_pM(t)$ that is transverse to the tangent bundle of $M(t)$. Using this fact, we will compute $\sigma(p,t)$ with respect to the bundle

$$\tilde{N}M(t) = \{(x,y,u,v)\in T_p\mathbb{R}^n\colon\ (x,y)\in M(t),\quad u=0\}.$$

The fiber $\tilde{N}_pM(t)$ of this bundle (based at the point $p=(x,y)\in M(t)$) is just an $(n-k)$-dimensional subspace of the v variable that is aligned with the y directions.

Under the change of coordinates

$$z = y - \varphi(x,t), \tag{14}$$

we obtain the transformed system

$$\begin{aligned}
\dot{x} &= f(x,z+\varphi(x,t),t), \\
\dot{z} &= g(x,z+\varphi(x,t),t) - \varphi_x(x,t)\,f(x,z+\varphi(x,t),t) - \varphi_t(x,t). \qquad (15)
\end{aligned}$$

The invariant manifold $M(t)$ now satisfies $z = 0$, and the bundle $\tilde{N}M(t)$ has been transformed into the normal bundle of $M(t)$ in the new coordinates. Indeed, the former $\{x = \text{const}, y \in \mathbb{R}^{n-k}\}$ subspaces have been mapped by (14) into the $\{x = \text{const}, z \in \mathbb{R}^{n-k}\}$ subspaces, which are now normal to $M(t) = \{(x, z) \in \mathbb{R}^n : z = 0\}$. We will compute $\sigma(x, t)$ with respect to the normal bundle of $M(t)$ in the transformed system (15).

To study small transverse perturbations to $M(t)$, we Taylor-expand the z equation of (15) in the z variable to obtain

$$\begin{aligned} \dot{x} &= f(x, z + \varphi(x,t), t), \\ \dot{z} &= \left[g_y(x, \varphi(x,t), t) - \varphi_x(x,t)\, f_y(x, \varphi(x,t), t)\right] z + O\Big(|z|^2\Big), \end{aligned} \tag{16}$$

with the subscripts referring to partial derivatives. Here we used the local invariance of $M(t)$, which implies

$$g(x, \varphi(x,t), t) = \varphi_x(x,t)\, f(x, \varphi(x,t), t) + \varphi_t(x,t).$$

To compute $\sigma(p, t)$, we first need to determine the linearized flow map DF_t^{t+s} featured in (3). Let $p = (x(t), z(t))$ denote the initial position of a trajectory $(x(t+s),\, z(t+s)) \in M(t+s)$ at $s = 0$. The linearized flow map DF_t^{t+s} is the fundamental matrix solution of the linearized system

$$\begin{aligned} \frac{d}{ds}\xi = {} & [f_x(x(t+s), \varphi(x(t+s), t+s), t+s) \\ & + f_y(x(t+s), \varphi(x(t+s), t+s), t+s)\, \varphi_x(x(t+s), t+s)]\, \xi \\ & + f_y(x(t+s), \varphi(x(t+s), t+s), t+s)\, z, \\ \frac{d}{ds}z = {} & [g_y(x(t+s), \varphi(x(t+s), t+s), t+s) \\ & - \varphi_x(x(t+s), t)\, f_y(x(t+s), \varphi(x(t+s), t+s), t+s)]\, z. \end{aligned}$$

The fundamental solution matrix to this system can be written as

$$DF_t^{t+s} = \begin{pmatrix} A_t(s) & B_t(s) \\ 0 & C_t(s) \end{pmatrix}, \qquad DF_t^t = I_{n\times n}, \tag{17}$$

where $A_t(s) \in \mathbb{R}^{k\times k}$, $B_t(s) \in \mathbb{R}^{k\times(n-k)}$, and $C_t(s) \in \mathbb{R}^{(n-k)\times(n-k)}$. Note that

$$\frac{d}{ds}C_t(s) = \Gamma(x(t+s), t+s) C_t(s),$$

with Γ defined in (9). Also note that

$$\left\| \Pi^{t+s}_{F_t^{t+s}(p)} DF_t^{t+s}\Big|_{N_pM(t)} \right\| = \|C_t(s)\| = \sqrt{\lambda_{\max}\left(C_t^T(s) C_t(s)\right)},$$

which implies

$$\begin{aligned} \sigma(p;t) &= \lim_{s\to+0} \frac{1}{s} \log \left\| \Pi^{t+s}_{F_t^{t+s}(p)} DF_t^{t+s}\Big|_{N_pM(t)} \right\| \\ &= \lim_{s\to+0} \frac{1}{2s} \log\left[\lambda_{\max}\left(C_t^T(s) C_t(s)\right)\right]. \end{aligned} \tag{18}$$

To compute (18), we now Taylor-expand $C_t(s)$ in s to obtain

$$\begin{aligned} C_t(s) &= I + \frac{d}{ds}C_t(0)s + \mathcal{O}\big(s^2\big) \\ &= I + \Gamma(x(t),t)s + \mathcal{O}\big(s^2\big), \end{aligned}$$

where we have used $C_t(0) = I_{(n-k)\times(n-k)}$ (cf. (17)). Using the notation $\lambda_{\max}[\,\cdot\,]$ for the maximal eigenvalue of a matrix, we then obtain

$$\begin{aligned} \sigma(p;t) &= \lim_{s\to+0}\frac{1}{2s}\log\left[\lambda_{\max}\left(C_t^T(s)C_t(s)\right)\right] \\ &= \lim_{s\to+0}\frac{1}{2s}\log\left\{\lambda_{\max}\left[I + \left[\Gamma^T(x(t),t) + \Gamma(x(t),t)\right]s + \mathcal{O}\big(s^2\big)\right]\right\} \\ &= \lim_{s\to+0}\frac{1}{2s}\log\left\{1 + \lambda_{\max}\left[\Gamma^T(x(t),t) + \Gamma(x(t),t)\right]s + \mathcal{O}\big(s^2\big)\right\} \\ &= \lambda_{\max}\left[\Gamma^T(x(t),t) + \Gamma(x(t),t)\right]/2, \end{aligned}$$

as claimed in statement (ii) of the theorem. ∎

5. Locating stable and unstable neighborhoods of $M(t)$. The normally stable and unstable subsets partition $M(t)$ into subsets in which infinitesimally small perturbations transverse to $M(t)$ start decaying or growing, respectively. The norm of such small perturbations is instantaneously constant on the boundary between $M_s(t)$ and $M_u(t)$.

As trajectories leave the vicinity of $M(t)$, the growth of their distance is no longer captured accurately by the linearized flow along $M(t)$. To locate finite-size neighborhoods of $M(t)$ where trajectories increase their distances from $M(t)$, we again assume that $M(t)$ is given locally in the form of a graph (7). As in the proof of Theorem 4, we use the change of coordinates

$$z = y - \varphi(x,t)$$

to transform $M(t)$ to the $z = 0$ plane. In the transformed coordinates, the flow satisfies

$$\begin{aligned} \dot{x} &= f(x, z+\varphi(x,t), t), \\ \dot{z} &= g(x, z+\varphi(x,t), t) - \varphi_x(x,t)\, f(x, z+\varphi(x,t), t) - \varphi_t(x,t). \end{aligned}$$

Taking the inner product of the second equation with z gives

$$\frac{1}{2}\frac{d}{dt}|z|^2 = \langle g(x, z+\varphi(x,t), t) - \varphi_x(x,t)\, f(x, z+\varphi(x,t), t) - \varphi_t(x,t), z\rangle.$$

The boundary between domains of instantaneous growth from, and decay to, the $\{z = 0\}$ plane is given by the *instantaneous stability boundary*

$$B(t) = \{(x,z) :\ \langle g(x, z+\varphi(x,t), t) - \varphi_x(x,t)\, f(x, z+\varphi(x,t), t) - \varphi_t(x,t), z\rangle = 0\}. \tag{19}$$

The stable and unstable neighborhoods of $M(t)$ are given by

$$\begin{aligned} S(t) &= \{(x,z) :\ \langle g(x, z+\varphi(x,t), t) - \varphi_x(x,t)\, f(x, z+\varphi(x,t), t) - \varphi_t(x,t), z\rangle < 0\}, \\ U(t) &= \{(x,z) :\ \langle g(x, z+\varphi(x,t), t) - \varphi_x(x,t)\, f(x, z+\varphi(x,t), t) - \varphi_t(x,t), z\rangle > 0\}. \end{aligned}$$

Note that

$$\begin{aligned}
&\langle g(x, z+\varphi(x,t),t) - \varphi_x(x,t)\, f(x, z+\varphi(x,t),t) - \varphi_t(x,t), z\rangle \\
&= \langle [g_y(x,\varphi(x,t),t) - \varphi_x(x,t)\, f_y(x,\varphi(x,t),t)]\, z, z\rangle + O\Big(|z|^3\Big) \\
&= |z|^2 \left[\left\langle \frac{1}{2}\left[\Gamma(x,t) + \Gamma^T(x,t)\right] e_z, e_z\right\rangle + O(|z|)\right]; \qquad (20)
\end{aligned}$$

therefore,

$$\begin{aligned}
M(t) \cap S(t) &= \left\{(x,z) : z = 0, \qquad \lambda_{\max}\left[\frac{1}{2}\left[\Gamma(x,t) + \Gamma^T(x,t)\right]\right] < 0\right\}, \\
M(t) \cap U(t) &= \left\{(x,z) : z = 0, \qquad \lambda_{\max}\left[\frac{1}{2}\left[\Gamma(x,t) + \Gamma^T(x,t)\right]\right] > 0\right\}.
\end{aligned}$$

As a result, we conclude that

$$\begin{aligned}
M_s(t) &\equiv M(t) \cap S(t), \\
M_u(t) &\subset M(t) \cap U(t).
\end{aligned}$$

Also note that by (19) and (20), both the instantaneous stability boundary $B(t)$ and the cylindrical surface

$$\mathcal{B}(t) = \{(x,z) :\ \sigma(x,t) = 0\} \qquad (21)$$

have the same intersection with the manifold $M(t)$. Therefore, near the manifold $M(t)$, the condition $\sigma(x,t) = 0$ gives an approximation to the instantaneous stability boundary $B(t)$; the error of the approximation grows linearly in the order of the distance from the manifold. This error can be decreased to quadratic in the distance if we also include the $O\big(|z|^3\big)$ term in (20) in our calculations. In that case, the calculated dividing surface $B(t)$ will have a quadratic tangency with $\mathcal{B}(t)$ along $M(t)$.

The instantaneous stability boundary $B(t)$ between stable and unstable neighborhoods of $M(t)$ can also be computed directly from (19) without Taylor expansion in the z variable. Specifically, for any fixed z value, we can locate the curve of x values satisfying (19). Putting all these curves together, we obtain the surface $B(t)$.

6. Applications. In each example below, an invariant manifold $M(t)$ is known to exist in the limit of a small parameter ϵ. We will continue the manifold for larger values of ϵ and apply Theorem 4 to identify normally stable and unstable subsets of $M(t)$. We then numerically verify the results on trajectories passing by $M(t)$.

6.1. Bubble dynamics in the wake of a cylinder. At a spatial location $\mathbf{x} \in \mathbb{R}^2$ and time t, let $\mathbf{u}(\mathbf{x}, t)$ denote the velocity of a two-dimensional incompressible fluid flow of density ρ_f. We denote the material derivative of the velocity field by

$$\frac{D\mathbf{u}}{Dt} = \frac{\partial \mathbf{u}}{\partial t} + (\boldsymbol{\nabla}\mathbf{u})\,\mathbf{u},$$

where $\boldsymbol{\nabla}$ denotes the gradient operator with respect to the spatial variable $\mathbf{x}$.

Let $\mathbf{x}(t)$ denote the path of a finite-size particle of density ρ_p immersed in the fluid with characteristic scale L. For spherical neutrally buoyant particles of radius $\alpha \ll L$, the Lagrangian particle velocity $\mathbf{v}(t)$ satisfies the Maxey–Riley equation of motion (cf. Maxey and Riley [11]; Benczik, Toroczkai, and Tél [2]; and Haller and Sapsis [8])

$$\begin{aligned} \dot{\mathbf{x}} &= \mathbf{v}, \\ \dot{\mathbf{v}} &= -\frac{1}{\epsilon}(\mathbf{v}-\mathbf{u}) + \frac{3R}{2}\frac{D\mathbf{u}}{Dt}, \end{aligned} \tag{22}$$

where $\epsilon = \frac{1}{\mu} \ll 1$ with the inertia parameter μ defined as

$$\mu = \frac{R}{St}, \quad R = \frac{2\rho_f}{\rho_f + 2\rho_p}, \quad St = \frac{2}{9}\left(\frac{\alpha}{L}\right)^2 \mathrm{Re},$$

with Re denoting the Reynolds number. The case $R < 2/3$ describes heavy particles, while $R > 2/3$ corresponds to bubbles; $R = 2/3$ corresponds to neutrally buoyant particles.

Note that (22) is of the form (8) with $x = \mathbf{x} \in \mathbb{R}^2$, $y = \mathbf{v} \in \mathbb{R}^2$, and

$$\begin{aligned} f(\mathbf{x},\mathbf{v},t) &= \mathbf{v}, \\ g(\mathbf{x},\mathbf{v},t) &= -\frac{1}{\epsilon}[\mathbf{v}-\mathbf{u}(\mathbf{x},t)] + \frac{3R}{2}\frac{D\mathbf{u}(\mathbf{x},t)}{Dt}. \end{aligned} \tag{23}$$

Haller and Sapsis [8] prove that for any fixed $\epsilon > 0$ small enough, (22) admits a globally attracting two-dimensional invariant manifold of the form

$$M(t) = \left\{(\mathbf{x},\mathbf{v}) \in \mathbb{R}^4 : \mathbf{v} = \mathbf{u}(\mathbf{x},t) + \epsilon\left[\frac{3R}{2} - 1\right]\frac{D\mathbf{u}(\mathbf{x},t)}{Dt} + \mathcal{O}(\epsilon^2)\right\}. \tag{24}$$

By comparison with the general form (7), formula (24) yields

$$\varphi(\mathbf{x},t) = \mathbf{u}(\mathbf{x},t) + \epsilon\left[\frac{3R}{2} - 1\right]\frac{D\mathbf{u}(\mathbf{x},t)}{Dt} + \mathcal{O}(\epsilon^2). \tag{25}$$

We apply Theorem 4 to identify the stable and unstable subsets of $M(t)$. Using (23) and (25), we obtain that the matrix $\Gamma(\mathbf{x},t)$ satisfies

$$\begin{aligned} \Gamma(\mathbf{x},t) &= [g_{\mathbf{v}} - \varphi_{\mathbf{x}} f_{\mathbf{v}}]_{\mathbf{v}=\varphi(\mathbf{x},t)} \\ &= \left[-\frac{1}{\epsilon}I - \varphi_{\mathbf{x}}\right] \\ &= -\frac{1}{\epsilon}I - \boldsymbol{\nabla}\mathbf{u}(\mathbf{x},t) + \mathcal{O}(\epsilon), \end{aligned}$$

and hence the NILE can be written as

$$\begin{aligned} \sigma(\mathbf{x},t) &= \lambda_{\max}\left[\Gamma^T(\mathbf{x},t) + \Gamma(\mathbf{x},t)\right]/2 \\ &= \lambda_{\max}\left[-\frac{1}{\epsilon}I - \frac{1}{2}\left(\varphi_{\mathbf{x}}(\mathbf{x},t) + \varphi_{\mathbf{x}}(\mathbf{x},t)^T\right)\right] \\ &= -\frac{1}{\epsilon}I + \frac{1}{2}\lambda_{\max}\left[\boldsymbol{\nabla}\mathbf{u}(\mathbf{x},t) + \boldsymbol{\nabla}\mathbf{u}(\mathbf{x},t)^T\right] + \mathcal{O}(\epsilon). \end{aligned}$$

Here we used the fact that by incompressibility of the flow, the two-dimensional symmetric matrix $\boldsymbol{\nabla}\mathbf{u}(\mathbf{x},t)+\boldsymbol{\nabla}\mathbf{u}(\mathbf{x},t)^T$ has zero trace; as a result, its eigenvalues have opposite signs.

Up to an order $\mathcal{O}(\epsilon)$ error, therefore, the stable and unstable subsets of $M(t)$ satisfy

$$M_s(t)\approx\left\{(\mathbf{x},\mathbf{v})\in M(t):\ \lambda_{\max}\left[\frac{\boldsymbol{\nabla}\mathbf{u}(\mathbf{x},t)+\boldsymbol{\nabla}\mathbf{u}(\mathbf{x},t)^T}{2}\right]<\frac{1}{\epsilon}\right\},$$

$$M_u(t)\approx\left\{(\mathbf{x},\mathbf{v})\in M(t):\ \lambda_{\max}\left[\frac{\boldsymbol{\nabla}\mathbf{u}(\mathbf{x},t)+\boldsymbol{\nabla}\mathbf{u}(\mathbf{x},t)^T}{2}\right]>\frac{1}{\epsilon}\right\}. \tag{26}$$

In other words, the manifold $M(t)$ becomes locally repelling over spatial regions where the largest rate of strain associated with the ambient flow field exceeds $1/\epsilon$. In these high-strain regions, inertial particle motions divert from motions generated by the reduced velocity field

$$\mathbf{v}=\mathbf{u}(\mathbf{x},t)+\epsilon\left[\frac{3R}{2}-1\right]\frac{D\mathbf{u}(\mathbf{x},t)}{Dt}+\mathcal{O}(\epsilon^2)$$

that governs particle motions on $M(t)$.

Due to the linear dependence of $f(\mathbf{x},\mathbf{v},t)$ and $g(\mathbf{x},\mathbf{v},t)$ on $\mathbf{v}$, the instantaneous stability boundary $B(t)$ turns out to coincide with the cylindrical surface $\mathcal{B}(t)$ defined in (21). Indeed, we have

$$\begin{aligned}
B(t)&=\{(\mathbf{x},\mathbf{z}):\ \langle-\left[\mathbf{z}+\varphi(\mathbf{x},t)-\mathbf{u}(\mathbf{x},t)\right]/\epsilon+3R\left(D\mathbf{u}(\mathbf{x},t)/Dt\right)/2,\mathbf{z}\rangle\\
&\qquad-\langle\varphi_x(\mathbf{x},t)\left(\mathbf{z}+\varphi(\mathbf{x},t)+\varphi_t(x,t)\right),\mathbf{z}\rangle=0\}\\
&=\{(\mathbf{x},\mathbf{z}):\ \langle-\mathbf{z}/\epsilon-\varphi_x(\mathbf{x},t)\,\mathbf{z},\mathbf{z}\rangle=0\}\\
&=\left\{(\mathbf{x},\mathbf{z}):\ \frac{1}{2}\left\langle\left[-\frac{I}{\epsilon}-\varphi_x(\mathbf{x},t)\right]\mathbf{z},\mathbf{z}\right\rangle+\frac{1}{2}\left\langle\left[-\frac{I}{\epsilon}-\varphi_x(\mathbf{x},t)\right]^T\mathbf{z},\mathbf{z}\right\rangle=0\right\}\\
&=\left\{(\mathbf{x},\mathbf{z}):\ |\mathbf{z}|^2\left[\left\langle\frac{1}{2}\left[\Gamma(\mathbf{x},t)+\Gamma^T(\mathbf{x},t)\right]e_z,e_z\right\rangle\right]=0\right\}\\
&\equiv\mathcal{B}(t).
\end{aligned}$$

To illustrate our results, we consider inertial particle motion in the von Kármán vortex street model of Jung, Tél, and Ziemniak [9]. Assuming incompressibility for the flow, we have a stream function $\Psi(x,y,t)$ from which the ambient fluid velocity field can be derived by letting $\mathbf{u}=(-\Psi_y,\Psi_x)$. Jung, Tél, and Ziemniak [9] propose to model the vortex stream with the stream function

$$\Psi(x,y,t)=f(x,y)\,g(x,y,t), \tag{27}$$

with

$$f(x,y)=1-\exp\left(-a^{-1/2}\left(\left(x^2+y^2\right)^{1/2}-1\right)^2\right). \tag{28}$$

Note that the flow satisfies the no-slip boundary condition at the cylinder surface given by $x^2+y^2=1$. The factor $a^{1/2}$ measures the width of the boundary layer. The factor g in (27)

models the contributions of the shed vortices and the background flow u_0 to the full flow. More specifically,

$$g(x,y,t) = -wh_1(t)\, g_1(x,y,t) + wh_2(t)\, g_2(x,y,t) + u_0 y s(x,y). \tag{29}$$

The first two terms in (29) describe the creation and evolution of two vortices of equal strength. The parameter w and the functions $h_i(t)$ represent the vortex strength and amplitudes, respectively. Because of the alternating behavior of the vortices, there is a constant phase difference of half period $T_c/2$ between the strength of the two vortices, i.e., $h_2(t) = h_1(t - T_c/2)$. For concreteness, we choose

$$h_1(t) = |\sin(\pi t/T_c)|. \tag{30}$$

Jung, Tél, and Ziemniak [9] assume the vortex centers move parallel to the x-axis at a constant speed:

$$x_1(t) = 1 + L\,[(t/T_c) \bmod 1], \qquad x_2(t) = x_1(t - T_c/2),$$
$$y_1(t) = -y_2(t) \equiv y_0.$$

The shapes of the vortices are governed by the factor

$$g_i(x,y,t) = \exp\left(-R_0\left[(x - x_i(t))^2 + \alpha^2\,(y - y_i(t))^2\right]\right),$$

with the characteristic vortex size $R_0^{1/2}$ and the aspect ratio parameter α.

Finally, the last term in (29) represents the contribution of the background flow of uniform velocity u_0. The factor

$$s(x,y) = 1 - \exp\left[-(x-1)^2/\alpha^2 - y^2\right]$$

accounts for the shielding of the background flow just behind the cylinder.

Following Benczik, Toroczkai, and Tél [2], we select the average vortex strength $w = 8 \times 24/\pi$; for inertia, we pick $\epsilon = 1/\mu = 3 \times 10^{-2}$; for particles, we pick bubbles with density ratio $R = 0.72$. In our computation of inertial particle trajectories, we use a 4th-order Runge–Kutta algorithm with absolute integration tolerance of 10^{-7}.

In Figure 4, we present two snapshots of the bubble dynamics projected from the full four-dimensional phase space to the three-dimensional space of $(x, y, |\mathbf{v}|)$. We show instantaneous images of the slow manifold $M(t)$ (blue surface) at four different times; red regions on $M(t)$ show the repelling subset $M_u(t)$ (computed from formula (26)) responsible for local instabilities on the slow manifold, while the semitransparent red cylinders show the stability surface $B(t)$. Colored dots indicate the current position of the bubbles in the space $(x, y, |\mathbf{v}|)$.

We release bubbles from a grey area of the phase space and track their evolution. The smaller inserts in Figure 4 show the distance $|\mathbf{z}| = |\varphi(\mathbf{x}, t) - \mathbf{v}|$ of the particles from the slow manifold (in these plots, therefore, the slow manifold $M(t)$ appears as a plane). Note that while all particles end up converging to the slow manifold, they are temporarily repelled by the red region $M_u(t)$, as predicted by our theory.

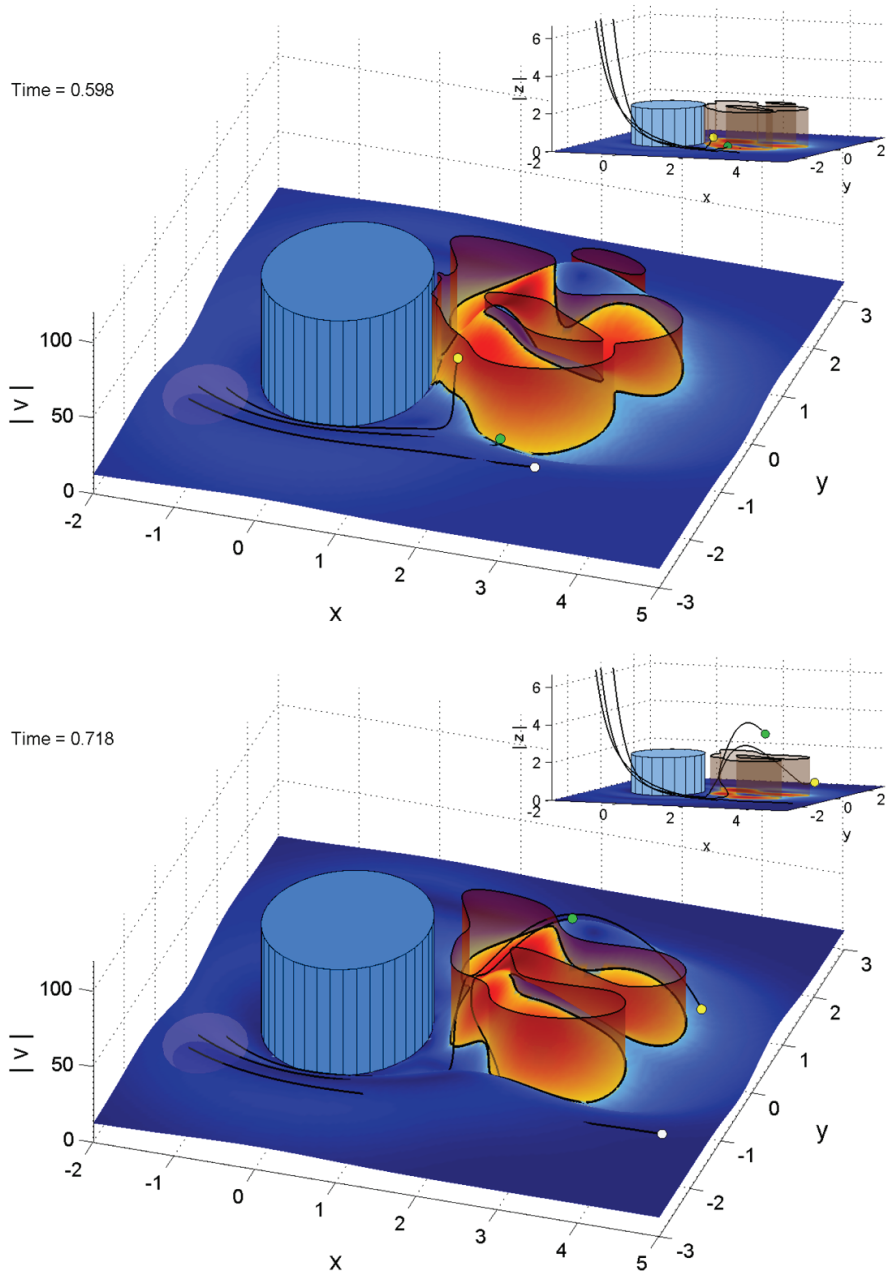

Figure 4. *Global convergence of bubbles to the inertial manifold $M(t)$, interrupted by local instabilities along the manifold. The red domains form the repelling subset $M_u(t)$ of the blue manifold $M(t)$ computed from the approximate formula* (26).

6.2. Spatially heterogeneous predator-prey interaction. Consider a predator-prey system where the prey can move freely between two spatial domains D_1 and D_2, while the predator must remain in domain D_1 (see, e.g., Poggiale and Auger [12] or Magal and Ruan [10]).

As a result, the prey population will have different growth rates over the two domains.

Let n_i be the prey density in domain D_i and let p denote the predator density. In each domain, the prey population growth rate and the predator population death rate are assumed to be linear; the predation rate is assumed to be proportional to both prey and predator densities; finally, the predator growth rate is taken to be proportional to the predation rate.

The resulting population model satisfies

$$\begin{aligned} \dot{n}_1 &= m_2 n_2 - m_1 n_1 + \epsilon n_1 (r_1 - ap), \\ \dot{n}_2 &= m_1 n_1 - m_2 n_2 + \epsilon n_2 r_2, \\ \dot{p} &= \epsilon p (b n_1 - d), \end{aligned} \tag{31}$$

where m_i is the proportion of prey population leaving domain i by displacement per unit time; r_i is the prey population growth rate on domain i; d is the predator population death rate; a is the predation rate on domain D_1; and bn_1 is the per capita predator growth rate. The small parameter $\epsilon \ll 1$ expresses the fact that spatial movements take place at a speed larger than that of the growth and death processes.

After letting $u_1 = \frac{n_1}{n}$ and $u_2 = \frac{n_2}{n}$, where $n = n_1 + n_2$ is the total amount of prey, we can rewrite system (31) as

$$\begin{aligned} \dot{u}_1 &= m_2 - (m_1 + m_2) u_1 + \epsilon u_1 (1 - u_1)(r_1 - r_2 - ap), \\ \dot{n} &= \epsilon n (r_1 u_1 + r_2 u_2 - a u_1 p), \\ \dot{p} &= \epsilon p (b u_1 n - d). \end{aligned} \tag{32}$$

Note that (32) is of the form (8) with $x = (n, p) \in \mathbb{R}^2$, $y = u_1 \in \mathbb{R}$, and

$$\begin{aligned} f(n, p, u_1) &= \begin{pmatrix} \dot{n} \\ \dot{p} \end{pmatrix} = \begin{pmatrix} \epsilon n (r_1 u_1 + r_2 u_2 - a u_1 p) \\ \epsilon p (b u_1 n - d) \end{pmatrix}, \\ g(n, p, u_1) &= \dot{u}_1 = m_2 - (m_1 + m_2) u_1 + \epsilon u_1 (1 - u_1)(r_1 - r_2 - ap). \end{aligned} \tag{33}$$

For $\epsilon = 0$, system (32) reduces to a classical Lotka–Volterra model. Additionally, as shown by Poggiale and Auger [12], the invariant manifold

$$M_0 = \left\{ (u_1, n, p) : u_1 = \frac{m_2}{m_1 + m_2} \right\}$$

is globally normally stable.

For sufficiently small $\epsilon > 0$, Fenichel's theorem on the persistence of normally hyperbolic invariant manifolds guarantees the existence of a globally attracting invariant slow manifold of the form

$$M_\epsilon = \{ (u_1, n, p) : u_1 = u_1(n, p) \}.$$

Magal and Ruan [10] show that M_ϵ satisfies

$$\varphi(n, p) \equiv u_1(n, p) = \frac{m_2}{m_1 + m_2} + \epsilon w_1(n, p) + \epsilon^2 w_2(n, p) + \mathcal{O}(\epsilon^3), \tag{34}$$

where

$$w_1(p) = \frac{m_1 m_2}{(m_1+m_2)^3}\,(r_1 - r_2 - ap),$$
$$w_2(n,p) = w_1(p)\,\frac{m_1 - m_2}{(m_1+m_2)^2}\,(r_1 - r_2 - ap) + ap\frac{m_1 m_2}{(m_1+m_2)^4}\left(\frac{bm_2 n}{m_1+m_2} - d\right).$$

Applying Theorem 4 gives the NILE in the form

(35)
$$\sigma(n,p) = -\left(m_1 + m_2 - \epsilon\left(1 - 2u_1(n,p,\epsilon)\right)(r_1 - r_2 - ap)\right) + \epsilon^2 abpn\frac{m_1 m_2}{(m_1+m_2)^3} + \mathcal{O}\left(\epsilon^3\right).$$

Using the notation $z = u_1 - u_1(n,p)$, we obtain the instantaneous stability boundary $B(t)$ (cf. (19)) in the form

$$\begin{aligned} B(t) &= \{(n,p,z):\ \langle g(n,p,z+\varphi(n,p)) - \varphi_{\mathbf{x}}(n,p)\,f(n,p,z+\varphi(n,p)), z\rangle = 0\} \\ &= \left\{(n,p,z):\ \left\langle \sigma(n,p)z - \epsilon z^2(r_1 - r_2 - ap), z\right\rangle = 0\right\} \\ &= \{(n,p,z):\ \sigma(n,p) - \epsilon z(r_1 - r_2 - ap) = 0\}. \end{aligned}$$

In Figure 5, we show the manifold M_ϵ for the parameter values $m_1 = 0.2$, $m_2 = 0.5$, $r_1 = 5$, $r_2 = 4$, $a = 3$, $d = 1$, $b = 1$, and $\epsilon = 0.2$ in the space (n,p,u_1) (top) and in the transformed space (n,p,z) (bottom). The coloring of the surface indicates the value of $\sigma(n,p)$, obtained by neglecting the $\mathcal{O}\left(\epsilon^3\right)$ terms in (35); red marks the normally unstable subset $M_u \subset M_\epsilon$, while blue marks $M_s \subset M_\epsilon$. In both figures we also show trajectories initiated over either M_u or M_s. Green dots indicate the initial condition for each trajectory.

As seen in Figure 5, most trajectories initialized over M_s converge monotonically to the manifold M_ϵ. One trajectory (ϑ_1 in Figure 5) performs a more complex motion: it temporarily enters the unstable domain U (and hence diverges from M_ϵ) and then re-enters the stable domain S to finally converge to M_ϵ. Similarly, for most trajectories initialized over the unstable domain M_u, we see a rapid initial divergence from the manifold. We also show an exception to this behavior: a trajectory (ϑ_2 in Figure 5) initiated close to the instantaneous stability boundary B leaves M_u, enters the stable region M_s, and starts converging to the manifold M_ϵ.

6.3. Soft-stiff mechanical systems. Georgiou, Corless, and Bajaj [5] study the dynamics of forced mechanical systems with a soft and a stiff component coupled in a nonlinear fashion. Their model is a two degree-of-freedom system with a stiff linear oscillator coupled to a soft oscillator with cubic nonlinearities (see Figure 6).

The equations of motion take the form

(36)
$$\begin{aligned} \dot{X}_1 &= X_2, \\ \dot{X}_2 &= (1+\beta)\left(X_1 - 2\zeta X_2 - \gamma X_1^3\right) + Y_1 + 2\rho Y_2, \\ \epsilon\dot{Y}_1 &= Y_2, \\ \epsilon\dot{Y}_2 &= -Y_1 - 2\rho Y_2 + \beta\left(-X_1 + 2\zeta X_2 + \gamma X_1^3\right), \end{aligned}$$

where $\beta = m_1/m$ is the mass ratio; $\gamma \equiv k_2/k_1$ is the normalized nonlinear spring coefficient; $\zeta = \delta_1/\left(2\sqrt{m_1 k_1}\right)$ and $\rho = \delta/\left(2\sqrt{mk}\right)$ are the linear damping factors for the linear and nonlinear spring; and, finally, $\epsilon = \sqrt{k_1 m/(k m_1)}$ is a small parameter describing the stiffness of the linear oscillator.

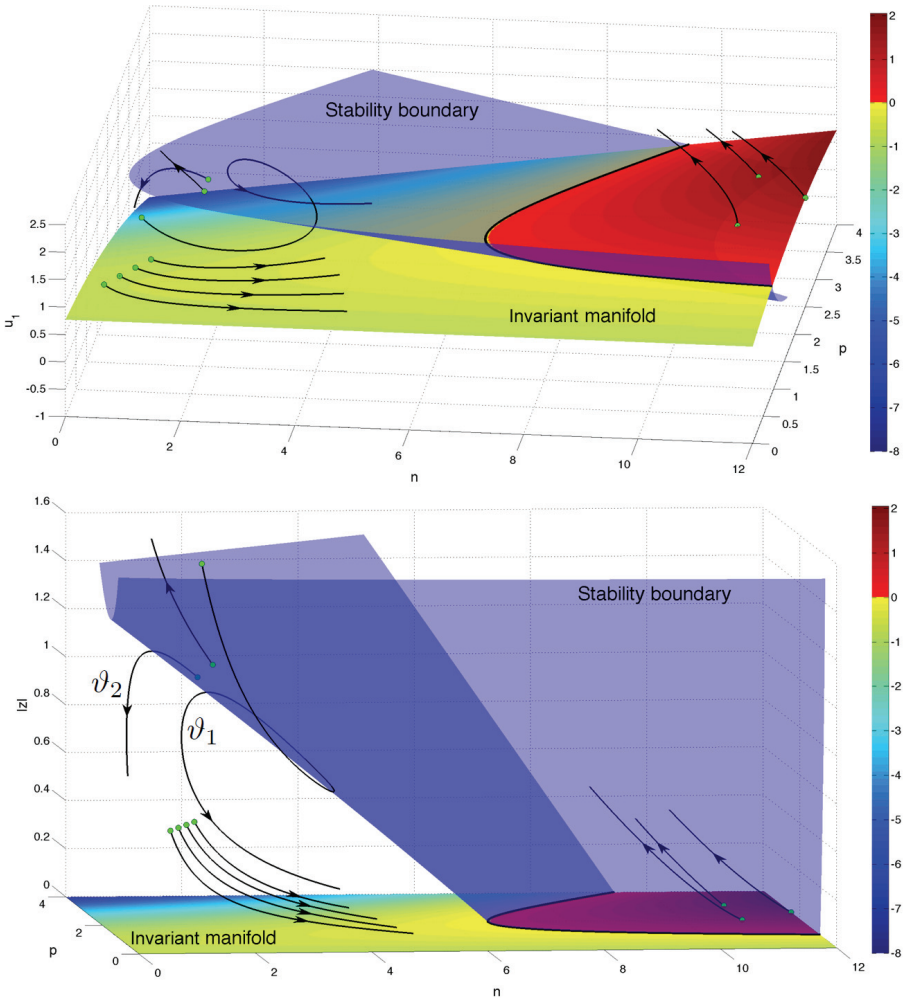

Figure 5. *The manifold M and the instantaneous stability boundary B in the original coordinates (n, p, u_1) (top) and in the transformed space (n, p, z) (bottom). The manifold M is colored according to the magnitude of $\sigma(n, p)$ for $\varepsilon = 0.2$. Shades of red: $\sigma(n, p) > 0$; shades of green: $\sigma(n, p) < 0$.*

We introduce the fast time $\tau = t/\epsilon$, which enables us to rewrite (36) as a regular perturbation problem of the form

$$
\begin{aligned}
X_1' &= \epsilon X_2,\\
X_2' &= \epsilon\left[(1+\beta)\left(X_1 - 2\zeta X_2 - \gamma X_1^3\right) + Y_1 + 2\rho Y_2\right],\\
Y_1' &= Y_2,\\
Y_2' &= -Y_1 - 2\rho Y_2 + \beta\left(-X_1 + 2\zeta X_2 + \gamma X_1^3\right).
\end{aligned}
\tag{37}
$$

For $\epsilon = 0$, this system admits an attracting manifold of fixed points given by

$$
\begin{aligned}
Y_1 &\equiv \varphi_{10}(\mathbf{X}) = \beta\left(-X_1 + 2\zeta X_2 + \gamma X_1^3\right),\\
Y_2 &\equiv \varphi_{20}(\mathbf{X}) = 0.
\end{aligned}
$$

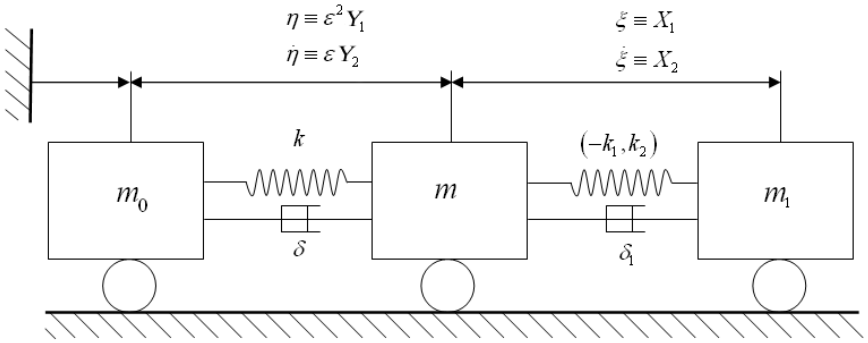

Figure 6. *Two degree-of-freedom soft-stiff mechanical system.*

By the results of Fenichel [4], for ϵ sufficiently small, the above system admits an attracting slow manifold, which Georgiou, Corless, and Bajaj [5] show to satisfy

$$M_\epsilon = \left\{ (\mathbf{X}, \mathbf{Y}) : \mathbf{Y} \equiv \begin{pmatrix} \varphi_1(\mathbf{X}) \\ \varphi_2(\mathbf{X}) \end{pmatrix} \right.$$
$$\left. = \begin{pmatrix} \varphi_{10}(\mathbf{X}) - 2\epsilon\rho H(X_1, X_2) + \epsilon^2 \left(4\rho^2 - 1\right) \beta W(X_1, X_2) \\ \epsilon H(X_1, X_2) - 2\epsilon^2 \rho\beta W(X_1, X_2) \end{pmatrix} + \mathcal{O}(\epsilon^3) \right\},$$

with

$$H(X_1, X_2) = \beta \left(3\gamma X_1^2 - 1\right) X_2 - 4\beta\zeta^2 X_2 - 2\beta\zeta \left(\gamma X_1^3 - X_1\right),$$
$$W(X_1, X_2) = \left(6\gamma X_1 X_2 + 2\zeta - 6\gamma\zeta X_1^2\right) X_2 + \left(3\gamma X_1^2 - 1 - 4\zeta^2\right) \left(-X_1 + 2\zeta X_2 + \gamma X_1^3\right).$$

Georgiou, Corless, and Bajaj [5] observe numerically that for larger ϵ values, the manifold M_ϵ undergoes qualitative changes and generates complex dynamics. More specifically, the manifold develops transverse instabilities, and hence the dynamics on the slow manifold no longer determines the asymptotic behavior of all solutions.

To identify the onset of local transverse instabilities for larger values of ϵ, we use Theorem 4. Noting that $x = \mathbf{X}$ and $y = \mathbf{Y}$ hold in the current example, we obtain the matrix Γ defined in (9) in the form

$$\Gamma(X_1, X_2) = \begin{pmatrix} \frac{\partial \varphi_1}{\partial X_2} & \frac{1}{\epsilon} + 2\rho \frac{\partial \varphi_1}{\partial X_2} \\ -\frac{1}{\epsilon} + \frac{\partial \varphi_2}{\partial X_2} & -\frac{2\rho}{\epsilon} + 2\rho \frac{\partial \varphi_2}{\partial X_2} \end{pmatrix}.$$

By Theorem 4, the NILE is equal to the largest singular value of $\Gamma(X_1, X_2)$, which satisfies the equation

$$\sigma(X_1, X_2) = \frac{\text{Trace } S(X_1, X_2)}{2} + \sqrt{\frac{[\text{Trace } S(X_1, X_2)]^2}{4} - \det S(X_1, X_2)}, \tag{38}$$

with $S(X_1, X_2) = \left[\Gamma(X_1, X_2) + \Gamma(X_1, X_2)^T\right]/2$.

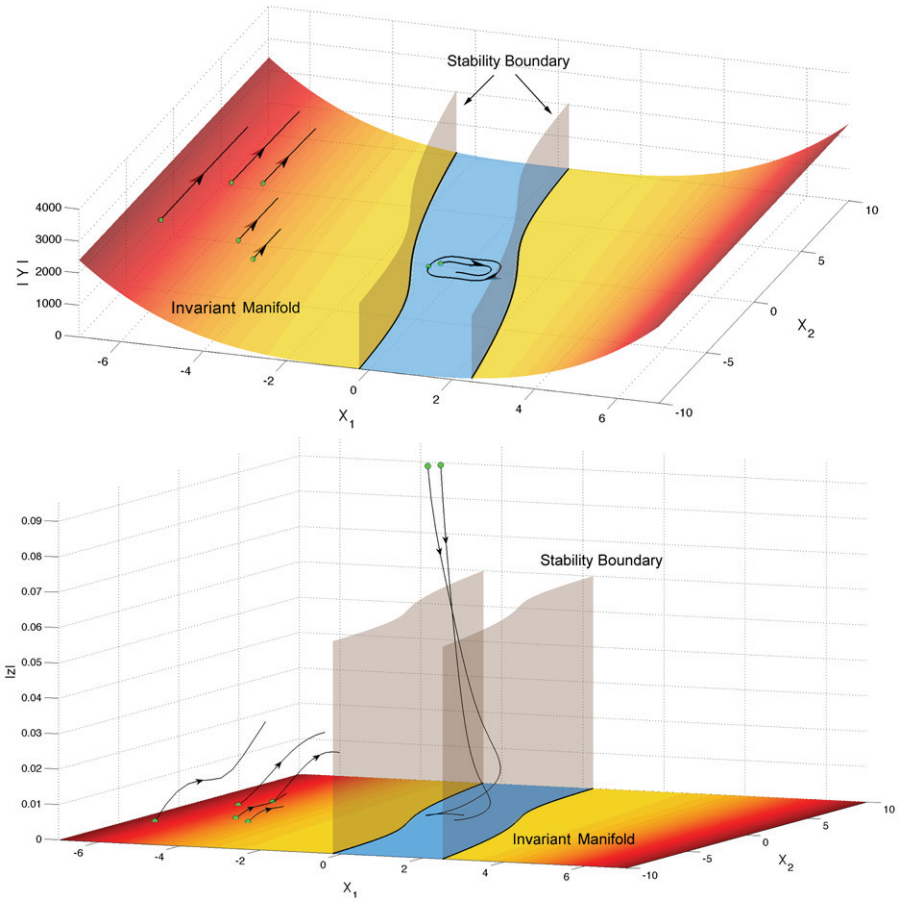

Figure 7. *Top: The invariant manifold M_ε in the physical space $(X_1, X_2, |Y|)$ for $(\beta, \gamma, \varepsilon) = (1, 7, 10^{-3})$ and $(\zeta, \rho) = \left(10^{-4}, 10^{-3}\right)$, with the domain of instability ($\sigma(X_1, X_2) > 0$) shown in red. Bottom: The invariant manifold M_ε in the transformed coordinate space $(X_1, X_2, |z|)$.*

Just as in our first example, the linear dependence of the system (37) on the fast variables (Y_1, Y_2) implies $B \equiv \mathcal{B}$. As a result, computing the curve $\sigma(X_1, X_2) = 0$ also gives us the instantaneous stability boundary in the full phase space.

Figure 7 (top) shows the invariant manifold M_ϵ in the coordinates X_1, X_2 and $|Y| = \left(Y_1^2 + Y_2^2\right)^{1/2}$ with coupling parameters $(\beta, \gamma, \epsilon) = (1, 7, 10^{-3})$ and dissipation factors $(\zeta, \rho) = \left(10^{-4}, 10^{-3}\right)$. Green dots indicate initial conditions for the trajectories shown. We observe that the above choice of system parameters results in a large stable neighborhood S for the invariant manifold. On the bottom plot, we also observe monotone convergence to the invariant manifold in the space of the variables X_1, X_2 and $|z| = \left((Y_1 - \varphi_1(X_1, X_2))^2 + (Y_2 - \varphi_2(X_1, X_2))^2\right)^{1/2}$ for trajectories inside the stable region S.

In Figure 8, the same system is shown with coupling parameters $(\beta, \gamma, \epsilon) = (1, 7, 10^{-1})$ and dissipation factors $(\zeta, \rho) = \left(0, 10^{-2}\right)$. In this case, the unstable region M_u covers a larger part of the manifold M_ϵ. However, the minimum eigenvalue of $S(X_1, X_2)$ is an order of magnitude larger than its maximum eigenvalue, $\sigma(X_1, X_2)$, and is globally negative, as can be deduced

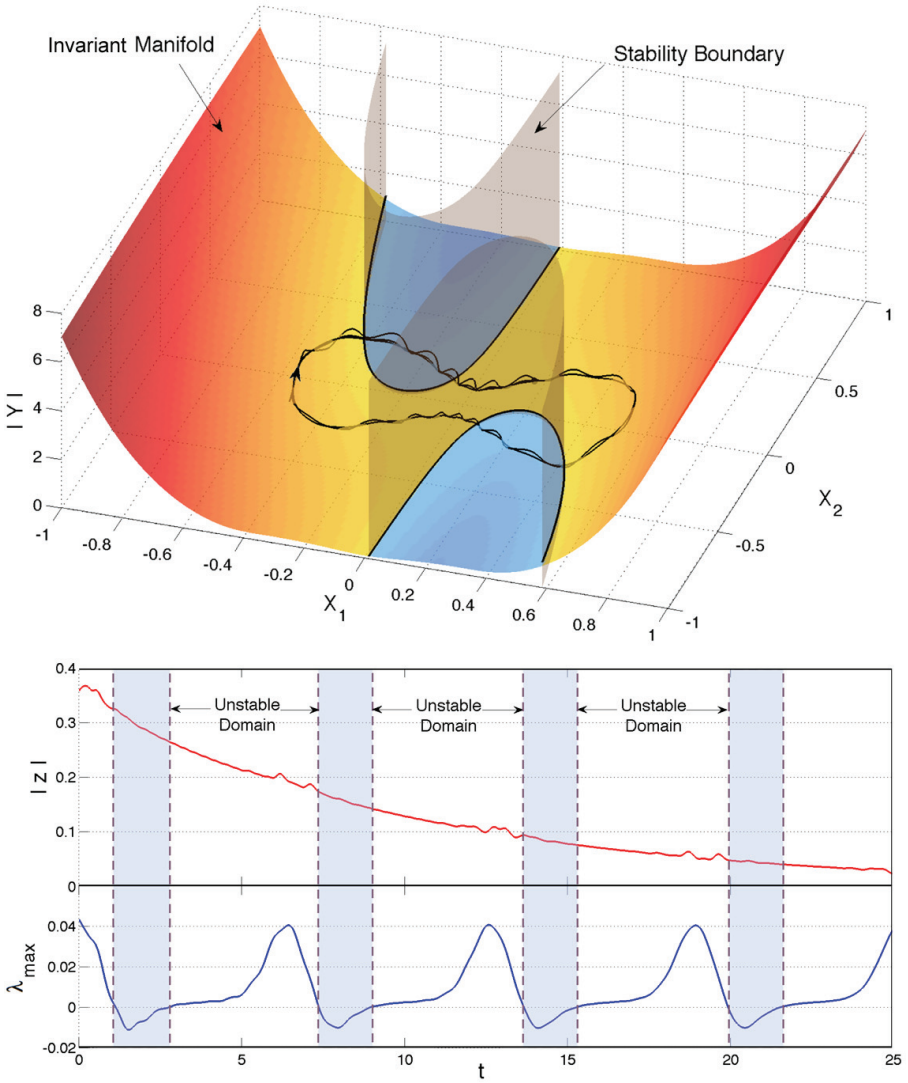

Figure 8. *Top: The invariant manifold M_ε for $\varepsilon = 0.1$ and $\rho = 10^{-2}$, with the domain of instability ($\sigma(X_1, X_2) > 0$) shown in red. Bottom: Time series of the distance from the slow manifold $|z(t)|$ (red curve) and the stability indicator $\sigma(\mathbf{X}(t))$ corresponding to the current position of the system (blue curve).*

from (38). As a result, entry of a trajectory into the unstable region manifests itself only in small perturbations away from the slow manifold, as opposed to the rapid divergence observed in previous examples. This is evidenced by the bottom plot of Figure 8 where the distance $|z(t)|$ (red curve) is shown together with $\sigma(X_1(t), X_2(t))$ (blue curve) along a trajectory of the system. The exponential decay of $|z(t)|$ is due to the minimal eigenvalue of $S(X_1, X_2)$ which has a large norm. This exponential decay is temporarily interrupted by smaller exponential growth while the trajectory is in the unstable neighborhood U of the slow manifold.

7. Conclusions. In this paper, we have defined the subsets $M_u(t)$ and $M_s(t)$ of an invariant manifold $M(t)$ as subsets that repel or attract nearby trajectories in directions normal to

$M(t)$. These domains exist independently of the stability type of the manifold. Indeed, a globally attracting invariant manifold may admit a normally unstable subset $M_u(t)$ that repels trajectories off the manifold while those trajectories stay in the vicinity of $M_u(t)$.

We have shown that if $\sigma(p,t)$ denotes the normal infinitesimal Lyapunov exponent (NILE) defined in (3), then the set $M_u(t)$ satisfies $\sigma(p,t) > 0$, while $M_s(t)$ satisfies $\sigma(p,t) < 0$. The NILE is a Lyapunov-type number that measures the instantaneous growth exponent of vectors transverse to $M(t)$ under the linearized flow along $M(t)$. Therefore, the NILE is the zero-time limit of growth exponents whose infinite-time limit is used in the theory of normally hyperbolic invariant manifolds to identify the long-term stability type of the manifold.

Our simple calculations show that unlike its infinite-time counterparts, the NILE is explicitly computable if the manifold is known in local coordinates. We have also derived an alternative form of the NILE that reveals its physical meaning as the maximal normal rate of strain along $M(t)$.

We have also derived an expression for the stable (unstable) neighborhoods of $M(t)$, which are sets of initial conditions whose distance from $M(t)$ decreases (increases) instantaneously. The boundary surface $B(t)$ between these two neighborhoods turns out to intersect $M(t)$ along the curve $\sigma(p,t) \equiv 0$.

The stable and unstable neighborhoods, as well as the normally stable and unstable subsets of $M(t)$, give a characterization of transient phenomena (such as jumps) near an invariant manifold. We have determined the geometry of these sets in three applications and used numerical simulations that confirm our results.

The simple geometric tools we have used in this paper do not allow us to conclude the existence of an invariant manifold. Rather, we assume that such a manifold exists and then determine its local stability properties. It seems likely, however, that the present approach can be used in locating invariant manifolds numerically or in predicting the limits of persistence of an invariant manifold under perturbations.

Acknowledgments. We thank Alexander Vakakis for suggesting the soft-stiff mechanical systems as an example. We thank the anonymous referees for their helpful comments and suggestions.

REFERENCES

[1] A. Babiano, J. H. E. Cartwright, O. Piro, and A. Provenzale, *Dynamics of a small neutrally buoyant sphere in a fluid and targeting in Hamiltonian systems*, Phys. Rev. Lett., 84 (2000), pp. 5764–5767.

[2] I. J. Benczik, Z. Toroczkai, and T. Tél, *Selective sensitivity of open chaotic flows on inertial tracer advection: Catching particles with a stick*, Phys. Rev. Lett., 89 (2002), 164501.

[3] N. Fenichel, *Persistence and smoothness of invariant manifolds for flows*, Indiana Univ. Math. J., 21 (1971), pp. 193–225.

[4] N. Fenichel, *Geometric singular perturbation theory for ordinary differential equations*, J. Differential Equations, 31 (1979), pp. 53–98.

[5] I. Georgiou, M. Corless, and A. Bajaj, *Dynamics of nonlinear structures with multiple equilibria: A singular perturbation-invariant manifold approach*, Z. Angew. Math. Phys., 50 (1999), pp. 892–924.

[6] G. Haller and G. Yuan, *Lagrangian coherent structures and mixing in two-dimensional turbulence*, Phys. D, 147 (2000), pp. 352–370.

[7] G. Haller, *Distinguished material surfaces and coherent structures in three-dimensional fluid flows*, Phys. D, 149 (2001), pp. 248–277.

[8] G. Haller and T. Sapsis, *Where do inertial particles go in fluid flows?*, Phys. D, 237 (2008), pp. 573–583.
[9] C. Jung, T. Tél, and E. Ziemniak, *Application of scattering chaos to particle transport in a hydrodynamical flow*, Chaos, 3 (1993), pp. 555–568.
[10] P. Magal and S. Ruan, eds., *Structured Population Models in Biology and Epidemiology*, Springer-Verlag, Berlin, Heidelberg, 2008.
[11] M. R. Maxey and J. J. Riley, *Equation of motion for a small rigid sphere in a nonuniform flow*, Phys. Fluids, 26 (1983), pp. 883–889.
[12] J. C. Poggiale and P. Auger, *Impact of spatial heterogeneity on a predator-pray system dynamics*, C. R. Biol., 327 (2004), pp. 1058–1063.
[13] T. Sapsis and G. Haller, *Instabilities in the dynamics of neutrally buoyant particles*, Phys. Fluids, 20 (2008), 017102.